1. Analysis of the two-dimensional photon echo (2DPE) data and coherent beats for PC645

1.1 Introduction

Analysis of the oscillations in 2DPE spectra was carried out on the total signal, as well as each of the rephasing and non-rephasing contributions to the total signal. The measurement of rephasing and non-rephasing spectra was achieved experimentally by reversing the order of arrival of the first two pulses at the sample. The non-rephasing spectra are associated with the $\tau<0$ pulse sequence and represent the free induction decay signals. On the other hand, the rephasing spectra are associated with the $\tau>0$ pulse sequence, involving rephasing of induced dipoles in an inhomogeneously broadened distribution (the photon echo). The photon echo causes a partial cancellation of the inhomogeneous broadening, therefore the rephasing pulse sequence give rise to stronger signals than the free induction decay signals generated by the non-rephasing pulse sequence.[3] We found that the ratio of rephasing and non-rephasing signal amplitudes is 3.6 at $T = 0$ and 2.9 at $T = 600$ fs.

It was recently demonstrated that separating rephasing and non-rephasing contributions is particularly useful in 2DPE spectroscopy in order to disentangle the complicated interference pattern that generates a 2D spectrum, and thereby clarify the exciton structure.[1] It was also demonstrated that the coherence pathways giving rise to quantum beats in 2DPE spectra have different contributions in the rephasing and non-rephasing pulse sequence. In particular, it was shown that beats in the diagonal peaks are dominated by the non-rephasing contribution, whereas beats in the cross peaks are due to rephasing contributions.[2]

In the present work, all the three variants of 2DPE spectra (rephasing, non-rephasing and total signal) were considered and analyzed. We examined their absolute value, imaginary part, and real part. However, all the results and observations reported in the paper refer only to the total signal and rephasing contributions of the real parts of the signal (i.e. absorptive contributions), since the absolute value and the imaginary part did not show any noteworthy features relevant to the focus of this report. Cross-peak beats in the absolute value of the total and rephasing signal were nonetheless analyzed (see section 1.5) in order to rule out the presence of possible artifacts due to interference between negative and positive contributions in the real part of the signal.

The presence of quantum beats at the diagonal and cross-peak positions was verified plotting the amplitude of the signal at these positions as a function of the population time T. The obtained traces

were firstly analyzed by taking a Fourier Transform (FFT) to extract the frequencies of the oscillations. The FFT results showed the presence of at least four frequency components at about 250, 350, 550 and 900 cm^{-1} (Figure S1).

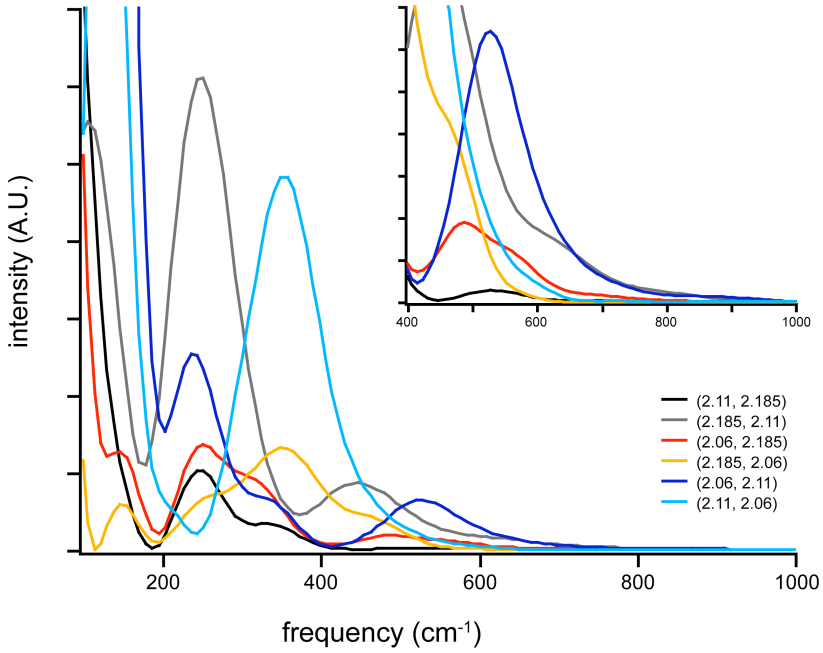

Figure S1. FFT analysis of the oscillating signal components at the cross peaks positions. The inset shows an enlargement of the high frequency region.

However, since the inverse of the Nyquist rate is comparable with our sampling time steps the FFT is not considered to be reliable. The same data were also analyzed fitting the amplitude traces with a sum of damped sine functions:

$$y = y_0 + \sum_{i=1}^{4} A_i \cdot \exp\left[-T/\tau_i\right] \cdot \sin\left(\omega_i T + \phi_i\right) \qquad \text{(S.1)}$$

where A_i, ω_i, ϕ_i and τ_i indicate the amplitude, angular frequency, phase and damping time constant of the i^{th} component (i=1–4).

This procedure allowed a more direct inspection of the damping times and the relative phase characterizing each frequency component and, in turn, a simpler interpretation of their physical meaning. In order to obtain meaningful fits, the following procedure was followed:

(i) The frequency values obtained with the Fourier Transforms were employed as first estimates of the fit parameters.

(ii) The amplitude traces at the significant cross-peak positions (see for example Fig. 2 in the text) were simultaneously analyzed with a global fitting procedure, allowing us to fit multiple datasets with one model simultaneously. Each frequency value was set as a shared (global) parameter and a single best-fit value was estimated.

(iii) The fit of each single scan was then individually optimized, keeping, where possible, the frequency values within a restricted interval around the global best-fit value previously found.

1.2. Real total signal

The real valued total 2DPE spectra show the presence of quantum beats both in diagonal and off-diagonal positions. The presence of this oscillation is evident also in a plot of the amplitude of the spectra along the diagonal and antidiagonal lines as a function of frequency and *T*. However, the broad line-widths, giving rise to closely entangled signals, results in a complicated and somewhat ambiguous analysis and interpretation of these oscillations. For this reason, oscillations in the rephasing and non-rephasing contributions were analyzed separately.

1.3. Real rephasing contribution (beats in cross-peaks)

The results obtained for fitting the intensity of the real-rephasing part of the 2D signal with eq. S.1 at the cross-peak positions are summarized in Figure S2 and Tables S1–S4.

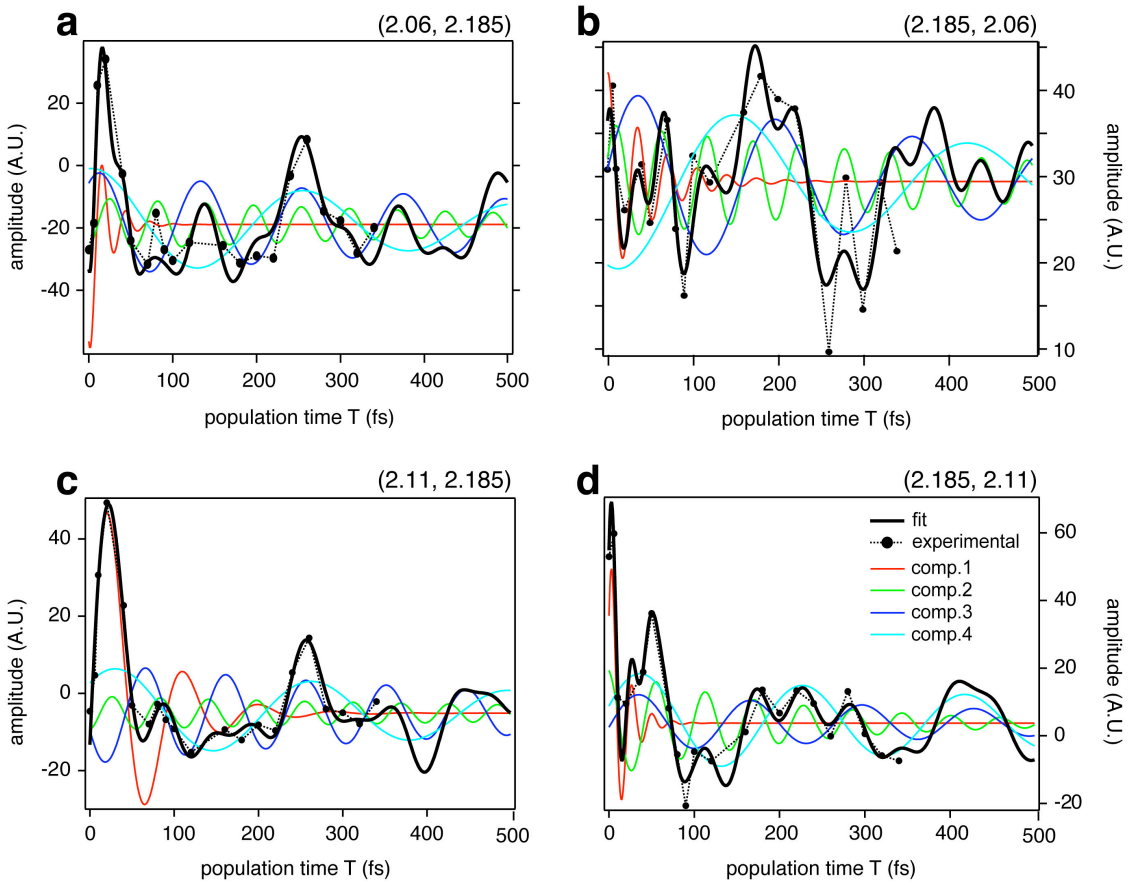

Figure S2. Comparison between the real, rephasing signal obtained from experimental data (circles and dotted line) and the fit using Eq. S.1 (thick black line) showing the intensity of four cross-peaks as a function of *T* for (a) the below-diagonal MBV-DVB cross peak; (b) the above-diagonal MVB-DVB cross peak; (c) the above-diagonal DVB_+-DVB_- cross peak; (d) the below-diagonal DVB_+-DVB_- cross peak. The thin colored lines represent the four frequency components extracted from the fits.

Table S1. Parameters from the fitting of the intensity of the below-diagonal DVB dimer cross peak at (2.185, 2.11).

i	A_i	ω_i (rad/fs)	ϕ_i	τ_i (fs)	ν_i (cm^{-1})
1	55.16	0.265	-5.67	16.94	**1405**
2	-16	0.109	23.8	204	**578**
3	8.9	0.048	-0.136	588	**254**
4	-15.4	0.033	-2.81	700	**175**
$y_0 = 3.74$					

Table S2. Parameters from the fitting of the intensity of the above-diagonal DVB dimer cross peak at (2.11, 2.185).

i	A_i	ω_i (rad/fs)	ϕ_i	τ_i (fs)	ν_i (cm^{-1})
1	76.16	0.0703	-6.38	57	**372**
2	4.42	0.110	23.79	700	**583**
3	13.05	0.066	-2.8	600	**350**
4	-12	0.027	-2.43	700	**143**
$y_0 = -5.13$					

Table S3. Parameters from the fitting of the intensity of the below-diagonal MBV-DVB cross peak at (2.185, 2.06).

i	A_i	ω_i (rad/fs)	ϕ_i	τ_i (fs)	ν_i (cm^{-1})
1	-11.16	0.18	4.56	50	**955**
2	-5.77	0.117	-2.47	500	**621**
3	7.34	0.05	-75.3	500	**265**
4	9.09	0.023	-8.23	500	**207**
$y_0 = 24.82$					

Table S4. Parameters from the fitting of the intensity of the above-diagonal MBV-DVB cross peak at (2.06, 2.185).

i	A_i	ω_i (rad/fs)	ϕ_i	τ_i (fs)	ν_i (cm^{-1})
1	43.88	0.222	-8.4	19	**1177**
2	8.59	0.110	-1.18	600	**583**
3	-16.8	0.052	-2.236	700	**276**
4	18.125	0.025	-74	500	**133**
y_0 = -18.9					

1.4. Real non-rephasing contribution (beats in diagonal peaks)

The results obtained from fitting the intensity of the real non-rephasing part of the 2DPE signal at the main diagonal peaks positions with eq. S.1 are summarized in Figure S3 and Tables S5–S7. We find that the oscillations seen in these plots are closely related to those of the cross-peaks in the real, rephasing signals. This observation is consistent with the predictions of Cheng and Fleming[2], which further strengthens the conclusions of our work.

Table S5. Parameters from the fitting of the intensity of the dimer DVB_+ diagonal peak at 2.185 eV.

i	A_i	ω_i (rad/fs)	ϕ_i	τ_i (fs)	ν_i (cm^{-1})
1	7.08	0.20	10.07	100	**1061**
2	14.50	0.12	-4.47	200	**637**
3	-3.22	0.067	2.14	500	**355**
4	8.34	0.038	-25.86	500	**202**
y_0 = -7.75					

Table S6. Parameters from the fitting of the intensity of the dimer DVB_ diagonal peak at 2.11.

i	A_i	ω_i *(rad/fs)*	ϕ_i	τ_i *(fs)*	ν_i *(cm^{-1})*
1	7.86	0.18	9.32	150	**955**
2	4.42	0.13	-4.50	500	**690**
3	-8.02	0.070	15.87	500	**371**
4	10.41	0.029	-17.47	500	**154**
$y_0 = 14.9$					

Table S7. Parameters from the fitting of the intensity of the MBV diagonal peak at 2.06.

i	A_i	ω_i *(rad/fs)*	ϕ_i	τ_i *(fs)*	ν_i *(cm^{-1})*
1	22.18	0.24	1.01	15	**1273**
2	2.25	0.104	4.75	500	**552**
3	6.86	0.073	-2.43	500	**387**
4	15.81	0.038	15.6	500	**202**
$y_0 = -0.83$					

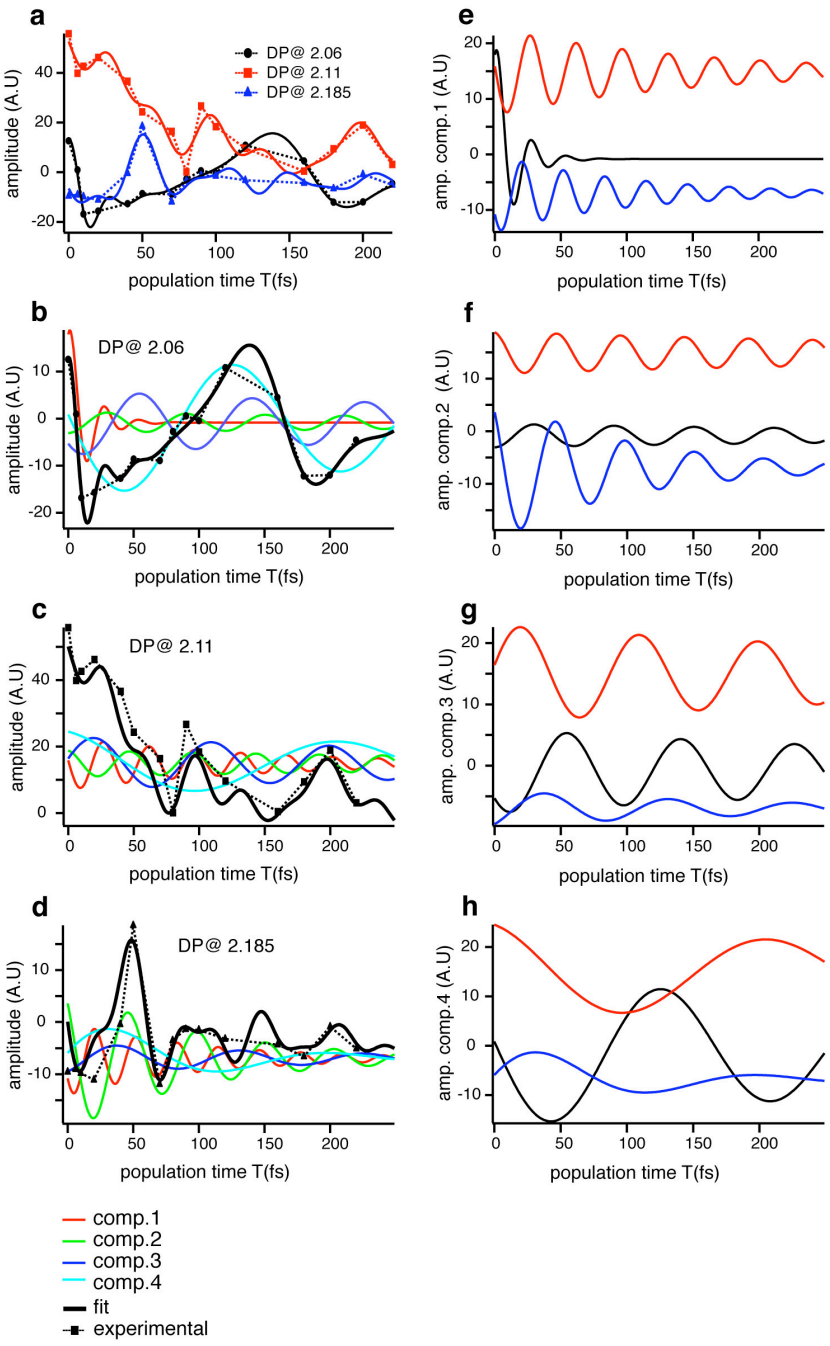

Figure S3. Real, non-rephasing signal contributions. (a) Intensity of the main diagonal peaks as a function of population time *T*: MBV @ 2.06 eV (black circles); DVB_- @ 2.11 eV (red squares) and DVB_+ @ 2.185 eV (blue triangles). Symbols and dotted lines represent experimental data, whereas the solid lines represent the fits. (b-d) Experimental data (symbols and dotted lines) and fits (thick black lines) for the three diagonal peaks showing also the four frequency components extracted from the fits (colored lines). In panels (e-h) each component (panel e=comp.1; panel f=comp.2;...) of the three diagonal peaks (MBV@2.06= black; DVB_-@2.11= red; DVB_+@2.185=blue) are compared to highlight the phase relationships of the oscillations.

1.5 Absolute values

The presence of cross-peak beats was recorded also in absolute value spectra of the rephasing (Fig. S4) and total (Fig. S5) signals. These beats are characterized by smaller amplitude than the beats in the real part spectra and they show somewhat more complicated behavior as function of T owing to the contributions and interferences of several signal pathways. However, beats in the cross-peaks at corresponding above and below diagonal positions still maintain the characteristic anticorrelation relationship typical of electronic coherences. The presence of such anticorrelated oscillations also in the absolute value cross-peaks amplitude shows that possible artifacts in the analysis of the real signal contributions due to the intersection of positive and negative signals are unlikely.

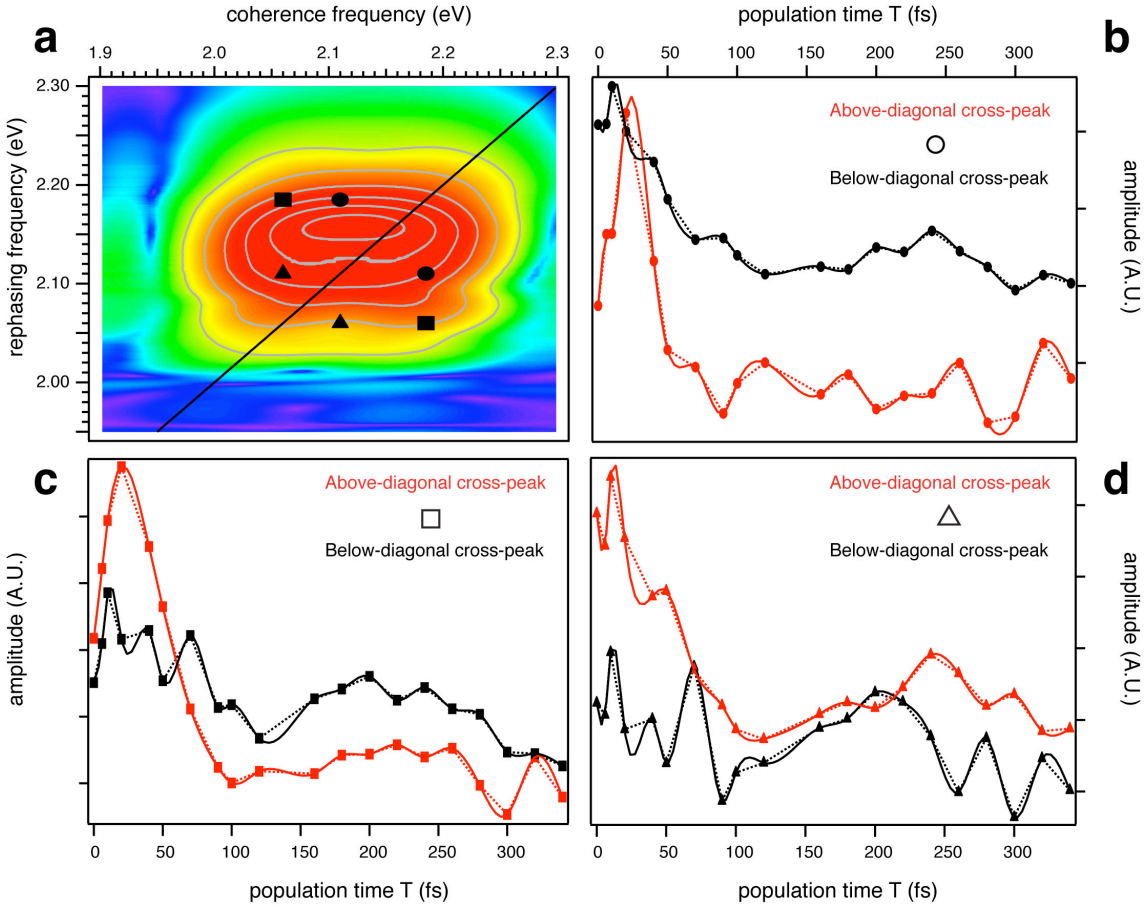

Figure S4. Absolute value of the rephasing contribution to the signal. (a) 2DPE spectrum for PC645 recorded at T = 20 fs showing the position of the off-diagonal peaks. (b-d) Intensity of the cross peaks as a function of T.

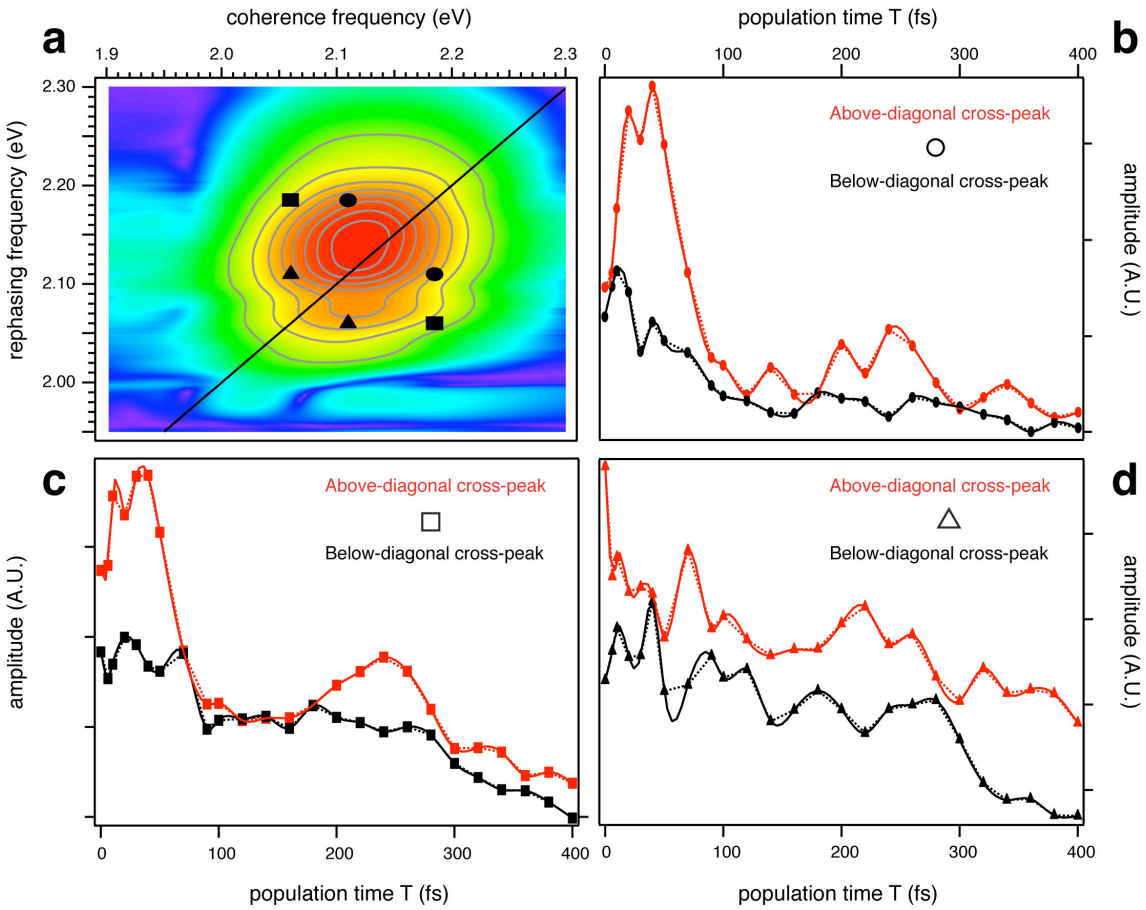

Figure S5. Absolute value spectra of the total signal. (a) 2DPE spectrum for PC645 recorded at T = 20 fs showing the position of the off-diagonal peaks. (b-d) Intensity of the cross peaks as a function of T.

2. Reproducibility

2.1 PC645 data

To prove that the analyzed oscillations are due to electronic quantum beats and not to experimental noise, we carefully checked the reproducibility of the 2DPE spectra:

(i) Each 2DPE map is the average of at least three separate scans.

(ii) At the end of each series of 2DPE scans at different T, a scan at the first T value was repeated to check the long time reproducibility. The decrease of the absolute value of the 2DPE signal was on average less than 15%, and the qualitative shape of the signal did not change within the experimental noise.

(iii) Each series of 2DPE scans at different T was further repeated several times on different days and on different solutions for comparison.

An example of different 2D spectra recorded at $T = 0$ on different days is reported in Figure S6.

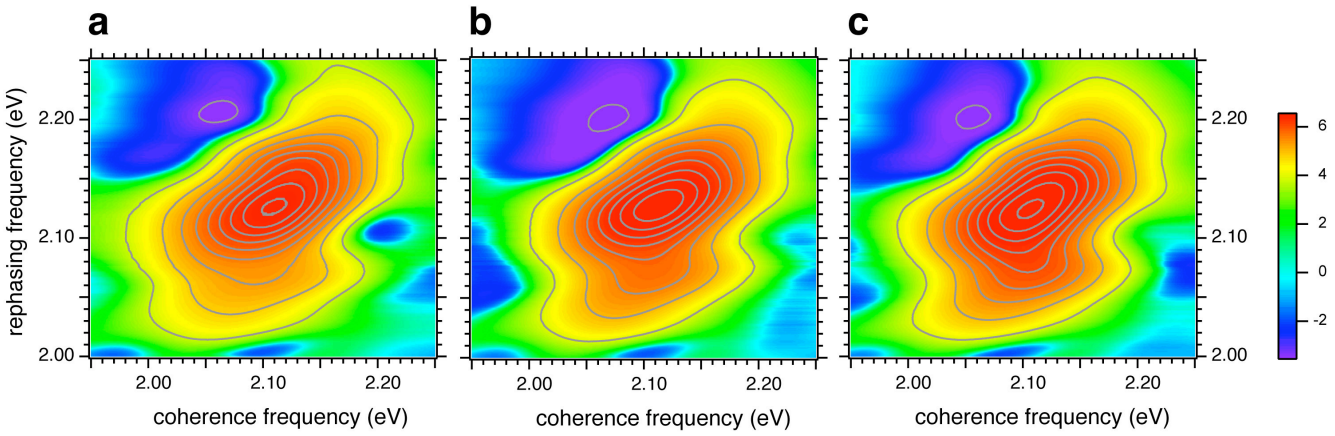

Figure S6. 2DPE spectra obtained at T=0 on different days (arcsinh color scale). Spectra (a) and (b) were recorded on the same solution, whereas spectrum (c) was measured for a freshly prepared solution. The spectra are not normalized and the difference in the absolute value of the intensity is less than 15%.

(iv) Each point of the traces showing the signal amplitude vs population time was then calculated as an average of at least four different scans. As an example, figure S7 shows the amplitude of the signal at the (2.06, 2.185) position (panel A, figure S2) with error bars calculated as standard deviations of repeated measurements during a single day.

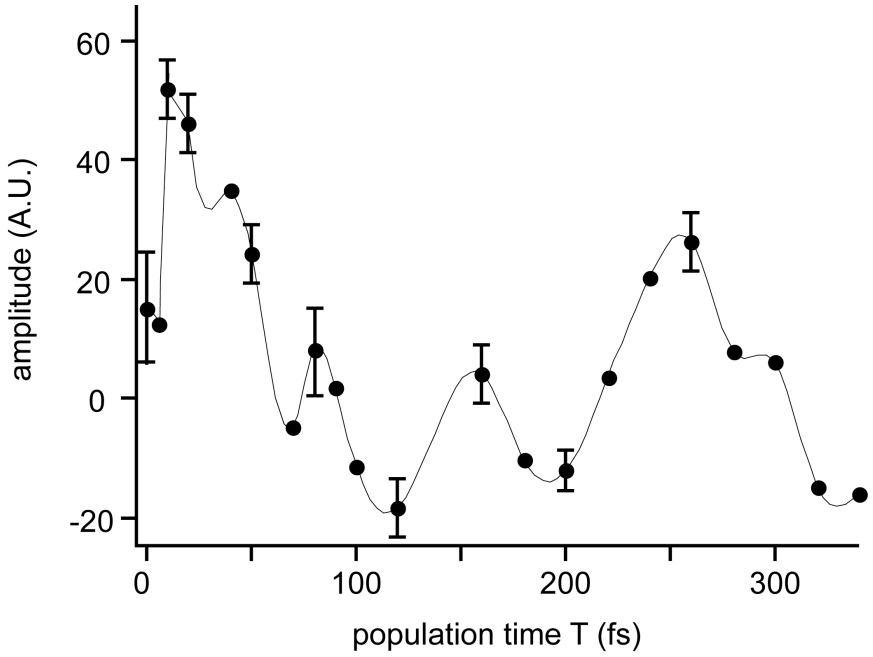

Figure S7. Amplitude of the signal at the (2.06, 2.185) position (see Fig.S2, panel A) as a function of *T*. Error bars are estimated as standard deviations of repeated scans on one day.

2.2 PE545 data

To ensure the quality of the PE545 data, the pulse characteristics were carefully monitored throughout the experiments. Transient grating frequency resolved optical gating (TG-FROG) measurements were performed on a solvent before and after the collection of each dataset to ensure that the pulse characteristics and alignment had not changed during the scan. Spectra of the local oscillator pulse were collected before and after the measurement of each population time (*T*) spectrum, to ensure that the pulse spectrum had not drifted, and to monitor the intensity of the laser pulse. The reproducibility of the data was tested by the collection of numerous datasets, each time using freshly prepared PE545 sample. The spectra were sometimes measured on different days, after realigning the laser table. Spectra were collected with different *T* ranges and using different *T* steps, and all confirmed the oscillations discussed in the paper. The real rephasing and non-rephasing results for three representative datasets using *T* steps of 10 fs are shown in Figure S8 and Figure S9 respectively. In order to minimize the contribution from minor fluctuations in laser power, the diagonal and anti-diagonal slices are normalized to the sum of the absolute value of the total signal. Since the power

fluctuations were quite small, as confirmed by the local oscillator spectra recorded between each T scan, this normalization procedure did not result in significant change in the appearance of the spectra.

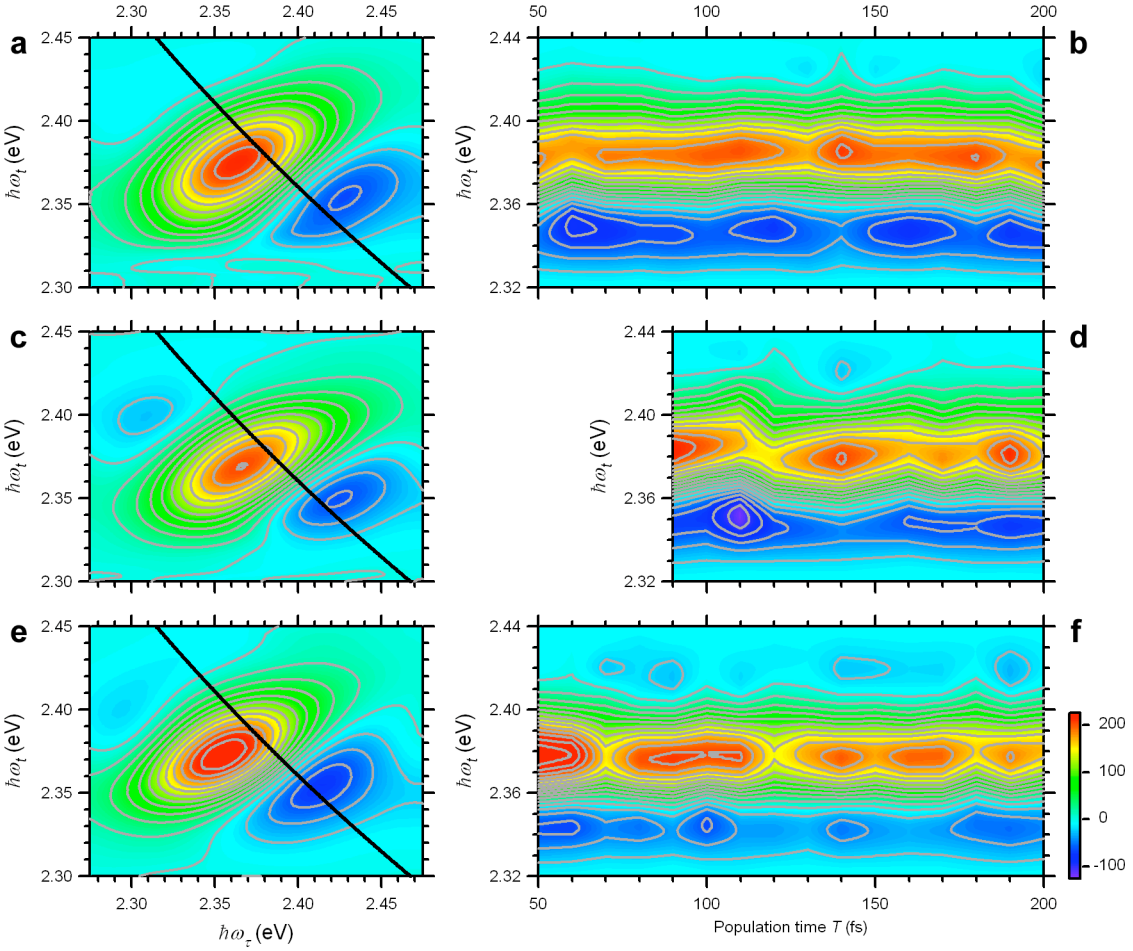

Figure S8. Rephasing real results for PE545, plotted on a linear intensity scale. (a) A spectrum collected at T=100 fs. (b) The intensity of the rephasing real spectra along an anti-diagonal slice through the cross-peaks, the black line in (a), as a function of population time (similar to Fig. 3(a) and 3(b)). Panels (c) thru (f) show the same results, each with freshly prepared PE545 samples, recorded on a different days.

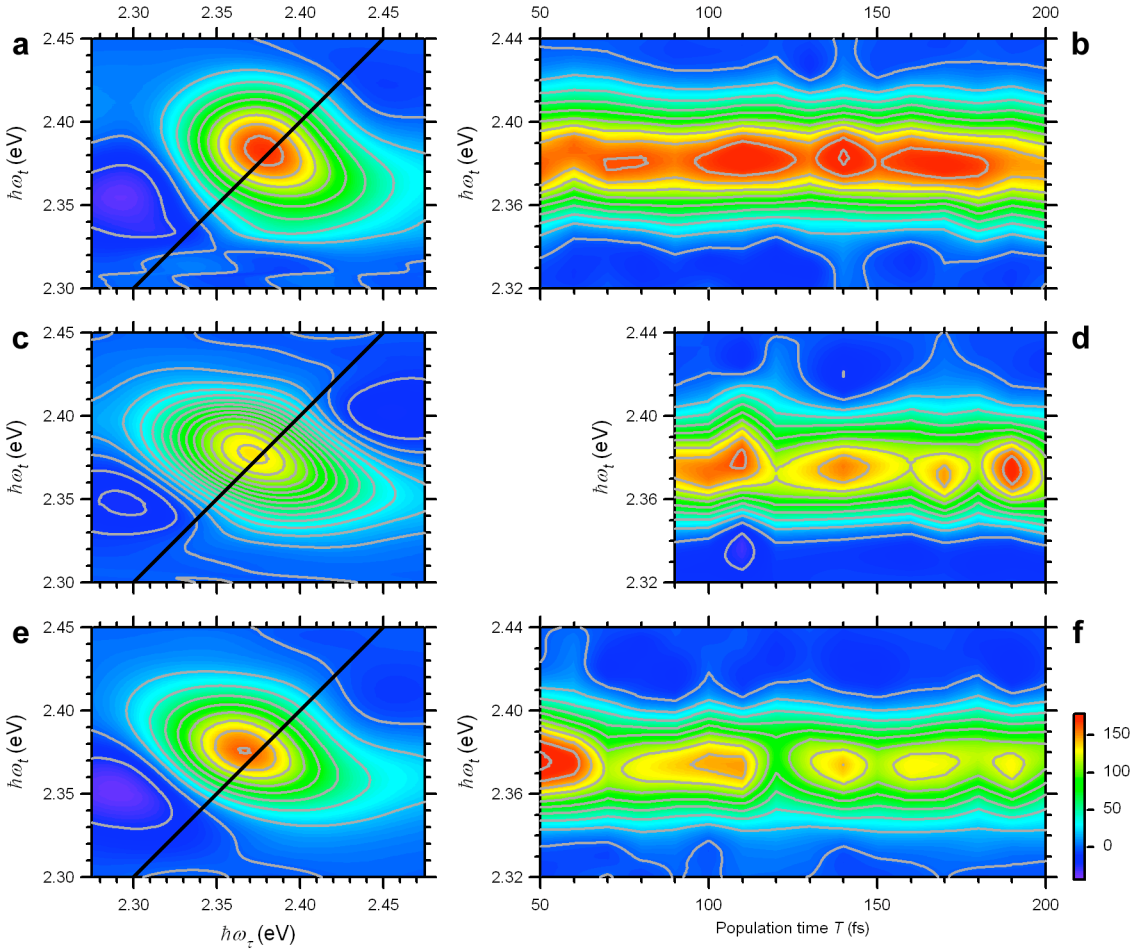

Figure S9. Non-rephasing real results for PE545, plotted on a linear intensity scale. (a) A spectrum collected at *T*=100 fs. (b) The intensity of the non-rephasing real spectra along a diagonal slice, the black line in (a), as a function of population time (similar to Fig. 3(d) and 3(e)). Panels (c) thru (f) show the same results, each with freshly prepared PE545 samples, recorded on a different days.

3. PC645 Structure

The center-to-center distances between molecules in the PC645 protein structural model are listed in Table S.8. The solvent-screened electronic couplings between pairs of molecules calculated using reasonably sophisticated quantum chemical methods, reported in Ref. 14 of the paper, are collected in Table S.9.

Table S.8. Distances between chromophores in PC645

PC645	α19A (MBV_A)	α19B (MBV_B)	β50/61C (DBV_C)	β82C (PCB_C)	β158C (PCB_C)	β50/61D (DBV_D)	β82D (PCB_D)
α19B(MBV_B)	46.3	-	-	-	-	-	-
β50/61C(DBV_C)	31.4	23.2	-	-	-	-	-
β82C(PCB_C)	33.9	24.9	22.5	-	-	-	-
β158C(PCB_C)	19.3	46.4	24.6	35.4	-	-	-
β50/61D(DBV_D)	23.5	31.1	15.2	31.6	21.2	-	-
β82D(PCB_D)	25.3	33.8	31.7	34.8	37.2	22.2	-
β158D(PCB_D)	46.3	19.2	20.6	36.9	41.9	24.0	35.0

Table S.9. Electronic couplings (meV) between chromophores in PC645

PC645	α19A (MBV_A)	α19B (MBV_B)	β50/61C (DBV_C)	β82C (PCB_C)	β158C (PCB_C)	β50/61D (DBV_D)	β82D (PCB_D)
α19B(MBV_B)	0.53	-	-	-	-	-	-
β50/61C(DBV_C)	–1.19	–5.44	-	-	-	-	-
β82C(PCB_C)	–1.96	6.76	–5.80	-	-	-	-
β158C(PCB_C)	–10.75	0.42	2.52	1.36	-	-	-
β50/61D(DBV_D)	5.44	0.94	39.60	2.67	3.78	-	-
β82D(PCB_D)	6.11	–1.82	–2.49	5.96	1.25	5.96	-
β158D(PCB_D)	–0.36	10.69	3.14	3.60	0.97	3.60	–1.33

References:

(1) Read, E. L.; Schlau-Cohen, G. S.; Engel, G. S.; Wen, J. Z.; Blankenship, R. E.; Fleming, G. R. *Biophys. J.* **2008**, *95*, 847.

(2) Cheng, Y. C.; Fleming, G. R. *J. Phys. Chem. A* **2008**, *112*, 4254.

(3) Mukamel, S. *Principles of Nonlinear Optical Spectroscopy*; Oxford University Press: New York, 1995.